Influence of molecular thermal motion on electronic excitation transport in anthracene crystals

Kohei Yokoi
Department of Instrumentation Engineering, Faculty of Science and Technology, Keio University, 3-14-1 Hiyoshi, Kohoku-ku, Yokohama 223, Japan
(Received 7 March 1991; revised manuscript received 10 September 1991)

Anisotropies in both the diffusion coefficient of triplet excitons and the mobilities of electrons and holes were numerically calculated in each direction of anthracene crystal axes at 95 and 290 K. Dynamic fluctuations of the molecular position, obtained by a molecular-dynamics simulation method, were used in *ab initio* calculations which determined the electronic excitation transport based on a hopping model. Compared with results from investigations considering only static perfect lattices, improvements were obtained in particular for the triplet exciton in the *ab* crystal plane and for the hole in all directions. However, as previously found in several studies, a discrepancy still remains between the theoretical and experimental anisotropies of the electron and triplet-exciton transport in the c' direction as compared with those in the *ab* plane. It is suggested this discrepancy is caused by static structural fluctuations, such as lattice defects in real crystals.

I. INTRODUCTION

It is believed that in a determination of the anisotropy and magnitude of the electronic excitation transport in molecular crystals not only the static perfect-lattice structure but also the molecular thermal motion should be considered. However, the inclusion of molecular motion is a difficult task because the dynamic fluctuations of the molecular position are large and complex, compared with those in atomic crystals, due to the weak intermolecular interactions and anisotropic molecular shapes.

The molecular wave functions for both the ground and lower excited states have small values at distances of about one van der Waals radius from the constituent atoms; thus intermolecular electronic overlaps are normally very small for a static perfect lattice having an energetically optimized molecular configuration. In the anthracene crystal at 300 K, however, the root-mean-square (rms) displacement of molecular location by thermal motion is ≈ 0.2 Å, and is not negligibly small compared with the shortest interatomic distance between molecules of ≈ 3 Å. Interatomic overlaps (a component of the intermolecular overlap) usually vary as $\exp(-\gamma r)$, where r is the interatomic distance and γ is a constant; hence the electronic overlap must be significantly influenced by the molecular thermal motion. This effect should then appear not only as fluctuations of the transfer rate, but also as a shift of the mean value originating in the asymmetry of the overlap integral with respect to the interatomic displacement from the equilibrium position. It is subsequently assumed that the intermolecular excitation transfer will take place at the moment that the molecular configuration becomes ready for the transport, i.e., when the transfer integral becomes large.

Transfer integrals are comprised of many intermolecular atomic integrals and are difficult to estimate analytically. The present paper therefore uses numerical analyses to study the anthracene crystal since it has been extensively studied both experimentally and theoretically. The previously calculated electron mobility for the static crystal lattice[1-4] did not correlate with the experimental results[5-8] in the c' direction until analytical attempts including molecular vibrations were employed: Gosar and Choi[9] failed to explain the anisotropy, using the idea that polarization relaxation occurs when a molecule is charged; Gosar and Vilfan[10,11] proposed the idea of phonon-assisted mobility; and Sumi[12] found that molecular rotational vibration is especially important for electron transport in the c' direction.

In contrast, for the triplet exciton, the anisotropy discrepancy concerning experimental[13-16] and theoretical[17-19] diffusion rates has not been explained, possibly as a result of the complex calculations which may be required to include charge-transfer states. The reason for this discrepancy, however, is expected to be similar to the case of the electron.

The present paper studies the transport of triplet excitons, electrons, and holes. The singlet exciton is excluded since the main transport contributor is not an intermediate-range interaction coming from the molecular orbital overlap, but instead a long-range dipole-dipole interaction. Analytical treatments of the molecular motion are difficult because of the large amplitudes and complex translational and rotational vibrations. In order to include molecular vibrations as rigorously as possible, a molecular-dynamics (MD) simulation was adopted instead of an analytical treatment involving uncertain approximation errors, and so the intermolecular electronic interactions are treated as being spatially and temporally dependent. However, lattice defects, which cause static fluctuations, are not considered in this paper.

Ab initio calculations were made for the transfer integrals, with the mobility and diffusion coefficient in each direction then being calculated by these integrals within the framework of a hopping model. Experimentally

determined mobility and diffusion coefficients were obtained as spatially and temporally averaged quantities within the simulation cell at simulation time.

II. MOLECULAR-DYNAMICS SIMULATION

Experimental data for crystal structures at 95 and 290 K were previously reported;[20] therefore simulations were conducted at these temperatures under the conditions of constant energy, volume, and molecular number. Since phase transition and defect generation are not of interest here, a constant-pressure simulation was not used in order to reduce the computing time. In addition, the unit-cell lattice constants were fixed at the experimentally observed values; Gear's predictor-corrector algorithm was used with quaternion parameters for angular representation, and the time step was 2 fs. The simulation time was taken as 10 ps after the thermal equilibrium state was established, and is believed to be adequate for molecular motion statistical analyses because of the short molecular translational and rotational vibration period (≈ 0.5 ps). The simulation cell consisted of 75 crystal unit cells (5, 5, and 3 units in the a, b, and c' direction, respectively) having 150 molecules. A periodical boundary condition was applied to the simulation cell.

The molecular potential was represented by the atom-atom potential method using Buckingham-type (6-exp) potentials with William's parameter set No. 4.[22] The anthracene molecule was treated as a rigid body with the dimensions measured by Cruickshank.[21] Two values were used for the CH bond length depending on the task at hand, i.e., the normal value of 1.08 Å for molecular moment-of-inertia calculations, and 1.027 Å (Ref. 22) for the potential calculation which considered the shift of the hydrogen atom's center of electron density. The molecular potentials of the excited states were approximated similar to those of the ground state since a preliminary simulation using the excited-state potential, estimated from the molecular polarizability, did not show an obvious difference in molecular motion from the ground-state potential. The cutoff distance of the atom-atom potential for all atom combinations was extended from 5–6 Å (Ref. 22) to 10 Å for any combination of atoms, and covers $\approx 95\%$ of the lattice energy. Further increases in the cutoff distance did not appear to affect the molecular motion in the coverage range. Coulomb interaction was not included because the contribution to the lattice energy is only 2.6% of the total.

Molecular-dynamics simulation results for the locational and orientational distributions are respectively shown in Figs. 1 and 2, being comparable to the experimental results[23] shown in Tables I and II. The ratios of the rms deviations at 290 and 95 K are ≈ 2 in all distributions, and the orientational symmetry of the two unit-cell molecules is equal to the experimental result expressed as the $P2_1/a$ space group, i.e., the Euler angles are in the relationship of $\theta_1+\theta_2=180°, \phi_1-\phi_2=180°$, and $\psi_1=\psi_2$. It should be noted that the symmetry was not retained by a lattice-energy optimization method using the quasi-Newtonian algorithm (i.e., a static method).[24] The MD simulation's qualitative and quantitative agreement with the experimental results is considered good enough to use for the subsequent electronic transport calculations.

III. ELECTRONIC EXCITATION TRANSPORT

The triplet-exciton diffusion coefficients and the electron and hole mobilities are calculated using two steps: (1) The transfer integrals between an excited (or ionic for the charge carriers) and a ground-state molecule are calculated using the intermolecular configuration obtained by the MD simulation, and (2) the excitation transfer rates which are based on a hopping (localized) model are

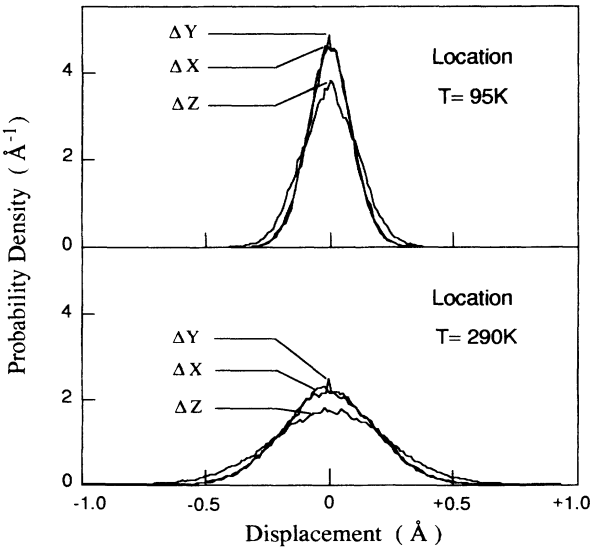

FIG. 1. Molecular location displacement at 95 and 290 K. ΔX, ΔY, and ΔZ are the deviations from the perfect crystal locations in the a, b, and c' directions, respectively.

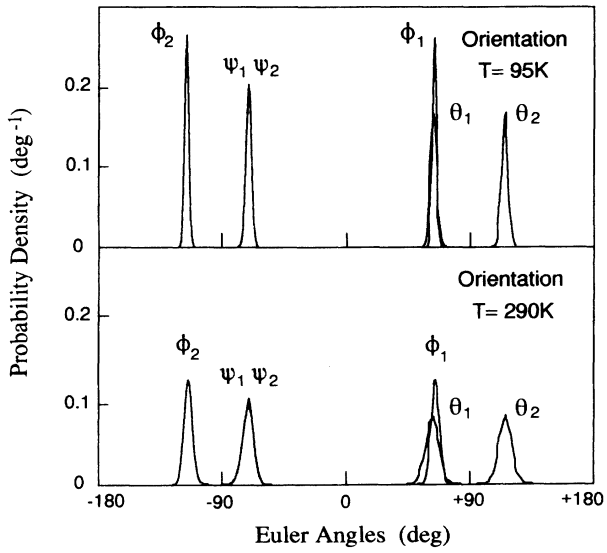

FIG. 2. Euler angles (θ,ϕ,Ψ) at 95 and 290 K. The subscripts 1 and 2 indicate the positions of the unit-cell molecules. The curves of Ψ_1 and Ψ_2 almost completely overlap each other.

TABLE I. Root-mean-square deviations of the molecular position. The values of ΔX, ΔY, and ΔZ are the calculated rms deviations of the location from the averages in the a, b, and c' directions, respectively, whereas ΔL, ΔM, and ΔN are experimental results (Ref. 23) in the respective directions of molecular axes L, M, and N, which are the long in-plane, short in-plane, and out-of-plane molecular axes, respectively. The symbols $\Delta\theta$, $\Delta\phi$, and $\Delta\Psi$ represent calculated rms deviations of Euler angles from the averages, while the symbols $\Delta\theta_L$, $\Delta\theta_M$, and $\Delta\theta_N$ (experimental results in Ref. 23) are, respectively, the orientational deviations with respect to the rotations around the molecular axes L, M, and N. Experimental results at ≈ 95 K are not available.

		Calculation			Experimental
		95 K	290 K		290 K
Location (Å)	ΔX	0.090	0.182	ΔL	0.197
	ΔY	0.089	0.189	ΔM	0.164
	ΔZ	0.112	0.227	ΔN	0.163
Orientation (deg)	$\Delta\theta$	2.36	4.72	$\Delta\theta_L$	3.82
	$\Delta\varphi$	1.55	3.06	$\Delta\theta_M$	2.24
	$\Delta\Psi$	1.99	3.90	$\Delta\theta_N$	3.10

calculated using the transfer integrals. The triplet-exciton diffusion is well described by a hopping model because of a narrow bandwidth on the order of ≈ 10 cm^{-1}. On the other hand, because the bandwidth is ≈ 100 times larger than that of the triplet exciton, charge transport was treated using both hopping and band models, i.e., it is in a region of applicability common to both models. In the present paper both these transports use a hopping model so as to phenomenologically and rigorously include molecular thermal motion.

The *ab initio* calculation of the transfer integrals is based on the methods of Jortner *et al.*,[17] and Tiberghien and Delacôte,[19] and the triplet exciton integral is the sum of exchange and charge-transfer interactions. The following is a summary of the method and assumptions used. Molecular wave functions are represented by a linear combination of ground-state carbon-atom self-consistent-field (SCF) $2p$ wave functions since all interactions are considered using the π-electron approximation. The transfer integrals consist of many intermediate-range interatomic integrals between molecules; thus the atomic wave functions are given by the sum of four Slater functions[25] which are accurate in the tail of the wave function. In contrast, the selection of linear combination of atomic orbital (LCAO) coefficients of atomic wave functions does not require such an accuracy, and the Hückel coefficients without overlap are accordingly employed. Both the nonorthogonality correction of the molecular wave functions between molecules and the three- and four-center integrals between different molecules were neglected because of the approximate nature of the calculation.

Based on Fermi's golden rule, the hopping model's local diffusion coefficient in the α direction at site i, $D_{i\alpha}$ (α is a, b, or c'), is expressed as

$$D_{i\alpha}=\frac{\pi}{\hbar}\sum_f\left[\frac{J_{if}^2R_{if\alpha}^2}{\sum_j J_{fj}}\exp\left[\frac{E_f-E_i}{kT}\right]\right]F \quad \text{for } E_f\geq E_i\ , \tag{1}$$

where J_{if} is the intermolecular transfer integral between the excited or the charged molecule at site i and a ground-state molecule at site f, $R_{if\alpha}$ is the α direction's cosine of the distance between the molecules, E_i and E_f are, respectively, the excitation energies of either the triplet exciton or the ionized energy levels for the charge carriers at sites i and f, k is the Boltzmann constant, T is the temperature, and F is the vibrational overlap factor for the molecular orbitals of interest, being considered constant regardless of molecular position. For the triplet exciton, F is the Franck-Condon factor between the vibrational ground states of the triplet state and either the ground or charge-transfer states, and was fixed at 0.25 for both states in accordance with experimental spectroscopic analyses[26] and calculations.[17,27] For the electron and

TABLE II. Euler angles of the molecular orientation. The symbols θ, ϕ, and Ψ are Euler angles (in degrees) of a molecule in the unit cell. The other molecule in the unit cell is in the relationship expressed by $P2_1/a$ space group. The calculated results are the orientations averaged over the simulation time and all molecules in the simulation cell. The experimental results are derived from the data on the direction cosines of the molecular axes with respect to the crystal axes (Ref. 23). The molecular orientation of $\theta=0°$, $\varphi=0°$, and $\Psi=0°$ is defined to that of the molecular L, M, and N axes equal to the crystal a, b, and c' axes, respectively.

	95 K		290 K	
Euler angles	Calc.	Expt.	Calc.	Expt.
θ (deg)	63.92	62.29	63.39	62.09
φ (deg)	63.98	65.22	65.01	66.33
Ψ (deg)	−70.86	−69.27	−71.44	−69.89

hole, F is the squared vibrational overlap between the ground states of a neutral molecule and a molecule charged by an electron or a hole. Although these F values are not accurately known they were set equal to the triplet-exciton value in order to get a rough estimate. If the excitation transport is from molecule i to f and $E_i < E_f$, the transfer rate must be multiplied by the Boltzmann factor corresponding to the energy difference. On the other hand, if an inverse energy relationship exists, there is no reduction using this factor. So when $E_f < E_i$, the Boltzmann factor is replaced by unity. Values of J, R, and E are all site and temporally dependent. The local diffusion coefficient is given by an averaged $D_{i\alpha}$ with respect to time. In addition, the density of state is uniform within the local bandwidth, $\sum J_{fj}$, where the surrounding molecules j are summed around the target molecule f.

The global diffusion coefficient in the α direction, D_α, is given by a spatial average of the local one as $D_\alpha = \langle D_{i\alpha} \rangle_i$, whereas the global mobility of the charge carriers in the α direction, μ_α, is conventionally expressed by Einstein's relation, i.e., $\mu_\alpha = \langle \mu_{i\alpha} \rangle_i = e \langle D_{i\alpha} \rangle_i / kT$, where e is the electron charge. The observable diffusion coefficient and mobility are respectively given by the time average of D_α and μ_α.

The diffusion coefficient is composed of the intermolecular electronic, vibronic, and Boltzmann parts, with all being dependent on the molecular configuration. The electronic part is simply obtained from the temporally dependent molecular configuration using the approximation that the molecular wave function is independent of the molecular environment. The vibronic part is probably approximated well as being constant even if intermolecular vibrations considerations are included. The molecular configuration fluctuations cause site-shift-effect and polarization fluctuations, thereby causing a fluctuation in the Boltzmann part.

The energies E_i and E_f are not only determined by the configurational relationship between the molecules i and f, but also by the neighboring molecules, i.e., over 30 molecules within the distance of about one unit cell. The spatial and temporal averaging therefore results in the Boltzmann factor being a constant factor B, hence Eq. (1) can be rewritten as

$$D_{i\alpha} = \frac{\pi}{\hbar} \sum_f \left[\frac{J_{if}^2 R_{ifa}^2}{\sum_j J_{fj}} \right] BF \ , \tag{2}$$

where B depends on the temperature and $0 < B < 1$. The use of this constant is the fundamental difference from the transfer integral case in which the interaction is primarily determined by only the i and j molecules. The Boltzmann factor is also discussed in Sec. IV. The estimation of the relative magnitude of the transports, i.e., $D_{i\alpha}/B$ and $\mu_{i\alpha}/B$ in each direction, is now the key to the comparison between theoretical and experimental transport investigations.

All previous discussions are valid for triplet-exciton and charge-carrier transport. However, if the crystal contains lattice defects, the fluctuation of the Boltzmann factor in these areas is not isotropic, and averaging the dynamic characteristics no longer results in a good approximation.

A. Triplet-exciton transport

The triplet-exciton transfer integral is comprised of the exchange and charge-transfer exciton interactions, with triplet- and charge-transfer-state energies being required to evaluate the latter contribution. For the triplet state an energy of 1.83 eV was taken,[28] while the energies of the charge-transfer states were derived from Coulomb's law for a dielectric continuum having a relative dielectric constant of 3.2 and a band gap fixed at the optical value of 4.4 eV, rather than the photoconductivity value of 4.1 eV.[29,30]

Transfer integral results are shown in Fig. 3, where the data are integrated with respect to space and time. Generally the values of exchange and charge-transfer interactions have different signs, thus the total value is distributed over a corresponding range. Main components of the transfer integral for the experimentally observed (static) structure are also shown for the exchange, charge-transfer, and total interactions. It should be noted that fine structures dependent on the crystal structure appear at 95 K but not at 290 K in the exchange and charge-transfer interactions. The local diffusion rate expressed as $D_{i\alpha}/B$ is widely distributed in each direction, as shown in Fig. 4. The anisotropy of the diffusion rate derived from $\langle D_{i\alpha}/B \rangle_i$ is shown in Table III along with other comparison data. By introducing molecular thermal motion, the calculated anisotropy is shown to correlate

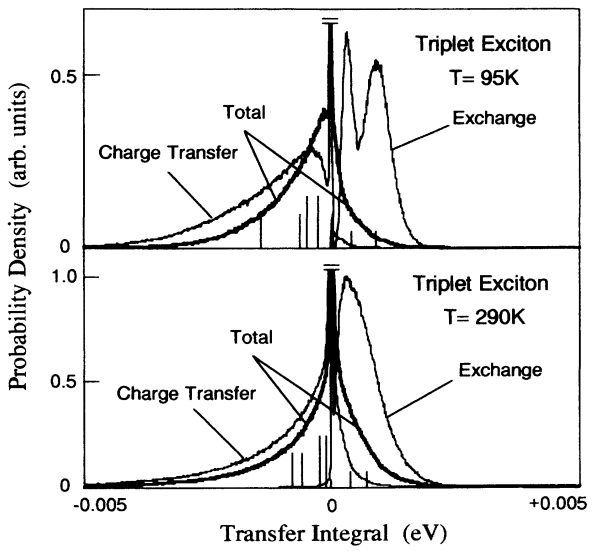

FIG. 3. Triplet-exciton transfer integrals. Distributions of the transfer integrals are shown for the exchange, charge-transfer, and total interactions. The short, middle, and long lines perpendicular to the abscissa axes, respectively, indicate the main components of the exchange, charge-transfer, and total interactions for the experimentally observed (static) structure. Many minor components at ≈ 0 eV are not shown. The sign of the integral was taken to be that valid under the C_2 point group.

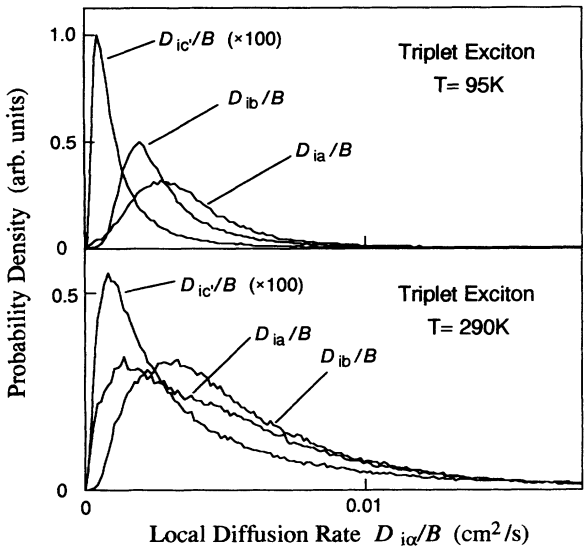

FIG. 4. The local diffusion rate $D_{i\alpha}/B$ of the triplet exciton in the a, b, and c' directions. The spatial average of $\langle D_{i\alpha}/B \rangle_i$ is 4.1×10^{-3}, 3.1×10^{-3}, and 0.015×10^{-3} cm²/s at 95 K, and 5.8×10^{-3}, 6.0×10^{-3}, and 0.049×10^{-3} cm²/s at 290 K for the a, b, and c' directions, respectively.

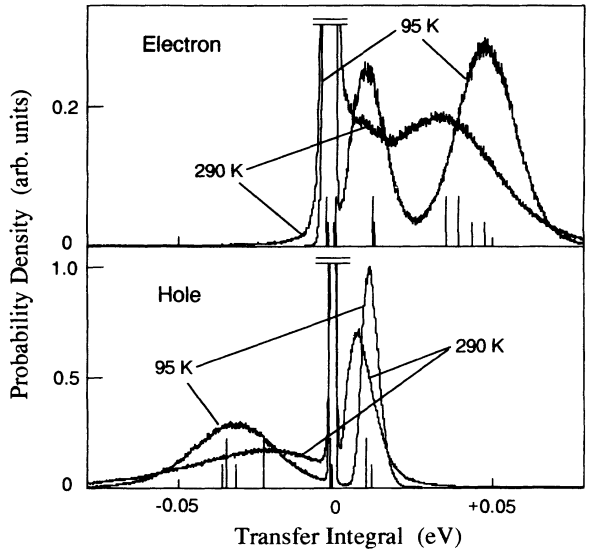

FIG. 5. Charge-carrier transfer integrals. The short and long lines perpendicular to the abscissa axes indicate main components of the integrals for the experimentally observed (static) structure at 95 and 290 K. Many minor components at ≈ 0 eV are not shown. The definition of the sign of the integral is the same as in Fig. 3.

well with the experimental results at 290 K in the ab plane; this is an expected result since the transfer integral is very sensitive to the molecular configuration. However, there is no improvement in the ratio of $D_{c'}/D_{ab}$, where D_{ab} is the diffusion rate in the ab plane given by $D_{ab}=(D_a+D_b)/2$ (see Sec. IV).

B. Electron and hole transports

In the present model, the highest occupied molecular orbital and lowest unoccupied molecular orbital of a neutral molecule influence the hole and electron transports, respectively. Transfer integrals of the electron and the hole are shown in Fig. 5, where the calculated integrals are distributed around the main components for the experimentally determined static crystal structures. The local mobility expressed as $\mu_{i\alpha}/B$ is distributed as shown in Fig. 6, with Table IV giving the anisotropy of the mobility derived from $\langle \mu_{i\alpha}/B \rangle_i$ and other comparison data. There are no discrepancies when compared with the experimental anisotropy of hole mobility since it is improved in the ab plane. However, in contrast, the electron still shows considerable discrepancy in $\mu_{c'}/\mu_{ab}$, being analogous to the case of the triplet exciton, although it is improved by a factor of 2 compared to the static analysis. This discrepancy was disappointing because it contradicts previous analytical predictions.[12]

IV. DISCUSSION

Molecular thermal motion was confirmed to play an important role in the electronic excitation transport in anthracene crystals; however, discrepancies arose between the calculated and experimental anisotropy found between the in-ab-plane and the c' direction for both the triplet-exciton diffusion rate and the electron mobility.

The most probable cause of this discrepancy is the presence of a number of lattice defects in the experimental crystals. Both the triplet-exciton and electron-transfer integrals in the c' direction are approximately 0.01 of those in the ab plane for perfect crystals; thus there is no doubt that the transfer rates in the c' direction increase with an increase in the lattice defect density, and also that the calculated anisotropy will get closer to the observed results. The defect density in melt-grown crys-

TABLE III. Anisotropy of the triplet-exciton diffusion rate.

	~95 K			~290 K		
	Dynamic	Static	Expt.[a]	Dynamic	Static	Expt.[b]
D_b/D_a	0.76	0.77		1.03	4.8	1.2
$D_{c'}/D_{ab}$[c]	0.0042	0.0036	0.075	0.0083	0.010	0.073

[a]Derived using only $D_a=0.40\times10^{-3}$ at 118 K (Ref. 13) and $D_{c'}=0.03\times10^{-3}$ cm²/s at 130 K (Ref. 15). Experimental data of D_b are unknown at $\approx$95 K.
[b]Derived from $D_a=0.15\times10^{-3}$, $D_b=0.18\times10^{-3}$, and $D_{c'}=0.012\times10^{-3}$ cm²/s at 298 K (Ref. 14).
[c]$D_{ab}=(D_a+D_b)/2$.

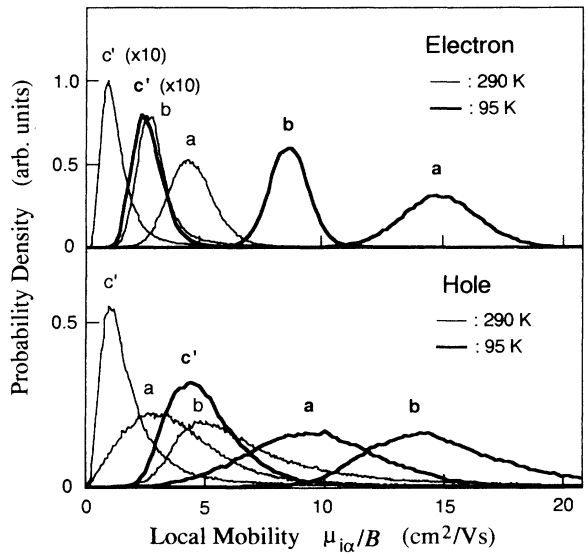

FIG. 6. The local mobilities of the charge carriers in the a, b, and c' directions. The spatial average of $\langle \mu_{i\alpha}/B \rangle_i$ for the electron is 13.6, 7.8, and 0.24 $cm^2/V\,s$ at 95 K, and 4.1, 2.7, and 0.13 $cm^2/V\,s$ at 290 K for the a, b, and c' directions, respectively, whereas for the hole, they are correspondingly 8.8, 13.8, and 4.7 $cm^2/V\,s$ at 95 K, and 3.9, 6.9, and 2.2 $cm^2/V\,s$ at 290 K.

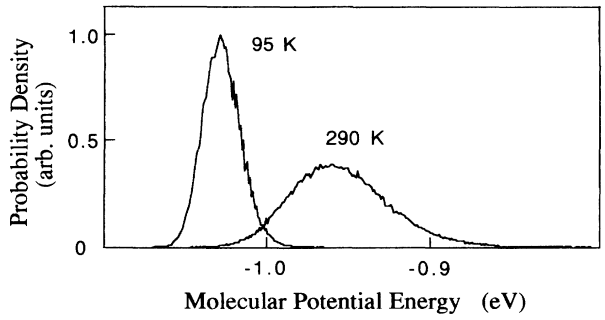

FIG. 7. Potential-energy distribution for the ground-state molecules.

tals was reported as 10^5-10^6 cm^{-2} for etch pits[33] and $\sim 10^{14}$ cm^{-3} for vacancies.[34] A more quantitative discussion is not presently possible since molecular arrangements around the lattice defects are not known and information concerning other types of lattice defects and impurities is not available.

The Eq. (2) Boltzmann factor, B, must be considered in order to compare the magnitude and temperature dependence of the calculated transport with the experimental results. Although it is difficult to exactly calculate this factor because of the difficulty of making a site-shift effect estimation, it can be estimated approximately using results from a supermolecule approach,[35] i.e., a relative molecular displacement of ≈ 0.2 Å (about the rms deviation produced by the thermal motion) in the out-of-plane direction for two molecules facing each other causes an energy-level shift of ≈ 0.0666 eV for the triplet excited state. If there is no effect from the other molecules, a Boltzmann factor of 0.07 is obtained (290 K) from the shift. On the other hand, based on the calculation and the experimental data, the expected factor, B, in the ab plane given by $(D_a+D_b)_{\rm calc}=(D_a+D_b)_{\rm expt}$ is ≈ 0.03. This is in fair agreement to the estimation and indicates that Eq. (2) is a good representation for the triplet exciton. When considering the charge carriers, however, appropriate methods to estimate the factor are unknown.

With respect to incorporating the temperature dependence of B into the presented method, the ratio of the width of the 95 and 290 K potential-energy distributions (Fig. 7) was determined to be 2.6. The energy distribution for the excited states was then assumed to be caused by an energy shift from the ground-state distribution without changing the probability distribution, and consequently the ratio of the average of E_f-E_i at the two temperatures was also taken as 2.6. Since the temperature ratio is 3.05, $B_{95\,\rm K}$ was taken as $B_{290\,\rm K}^{1.17}$ $(=3.05/2.6)$. If $B_{290\,\rm K}=0.03$, then it follows that $B_{95\,\rm K}=0.017$. Using this estimation of B, the temperature dependence of the triplet-exciton diffusion rate in the a direction would then be opposite to that observed in the experimental results. However, all other directionally averaged data obtained by various measurement methods[36-39] support the experimental results. This apparent discrepancy may be a result of the triplet-exciton transport being very sensitive to the molecular configuration as mentioned before, being subject to the strong influence of lattice defects and impurities which

TABLE IV. Anisotropy of the charge-carrier mobility.

		95 K			290 K		
		Dynamic	Static	Expt.[a]	Dynamic	Static	Expt.[b]
Electron	μ_b/μ_a	0.57	0.58		0.66	0.60	~0.50
	$\mu_{c'}/\mu_{ab}$[c]	0.022	0.019	0.05	0.038	0.021	~0.30
Hole	μ_b/μ_a	1.6	1.8		1.8	2.6	~1.8
	$\mu_{c'}/\mu_{ab}$[c]	0.42	0.42		0.41	0.41	~0.45

[a]Derived using only $\mu_a \sim 6.3$ (Ref. 5) and $\mu_{c'} \sim 0.34$ (Ref. 31) $cm^2/V\,s$ for the electron. The other experimental data at ≈ 95 K are unknown.

[b]Derived from $\mu_a \sim 1.8$, $\mu_b \sim 0.9$, and $\mu_{c'} \sim 0.4$ $cm^2/V\,s$ for the electron, and $\mu_a \sim 1.2$, $\mu_b \sim 2.1$, and $\mu_{c'} \sim 0.75$ $cm^2/V\,s$ for the hole (Refs. 5–8 and 32).

[c]$\mu_{ab}=(\mu_a+\mu_b)/2$.

become dominant at low temperatures.

Another possible factor which may cause discrepancies in the results is the lattice relaxation due to molecular excitations or ionizations. For the triplet-exciton transport, the lattice relaxation around the excited molecule will decrease the excited energy level and increase the transfer integral since the dispersion force of the excited molecule is greater than that of the ground-state molecule, thus being more attractive to the neighboring molecules. For the charge-carrier transport, the circumstance is almost similar, although the force comes from the polarization effect of the environmental molecules around the charged molecule. The decrease in the energy levels and the increase of the transfer integrals subsequently results in opposite effects on the transport, and so they more or less compensate each other. And even if the lattice relaxation is assumed to be faster than the excitation transports, the influence on the transport is not considered strong because the self-trap phenomena of the exciton and the charge carriers have not been observed in anthracene crystals under the atmospheric pressure.

Further studies will include lattice defects and lattice relaxations in the MD simulation in order to obtain better correlating results. These effects are believed to be more important than improving the transfer-integral calculations since the transfer integrals are very sensitive to the molecular position. It is realized this study considered only the anthracene crystal, but nonetheless the molecular thermal motion is believed to be important for estimating electronic excitation transport in other molecular solids. MD simulations are expected to be a useful tool because molecular motion at room temperature is large and too complex for analytic approaches in the determination of the excitation transport.

[1]O. H. LeBlanc, J. Chem. Phys. **35**, 1275 (1961).
[2]G. D. Thaxton and R. C. Jarnagin, J. Phys. Chem. **66**, 2461 (1962).
[3]J. I. Katz, S. A. Rice, S. I. Choi, and J. Jortner, J. Chem. Phys. **39**, 1683 (1963).
[4]R. Silbey, J. Jortner, S. A. Rice, and M. T. Vala, J. Chem. Phys. **42**, 733 (1965); **43**, 2925(E) (1965).
[5]R. G. Kepler, Phys. Rev. **119**, 1226 (1960).
[6]I. Nakada and Y. Ishihara, J. Phys. Soc. Jpn. **19**, 695 (1964).
[7]J. Fourny and G. Delacôte, J. Chem. Phys. **50**, 1028 (1969).
[8]G. T. Pott and D. F. Williams, J. Chem. Phys. **51**, 1901 (1969).
[9]P. Gosar and S. I. Choi, Phys. Rev. **150**, 529 (1966).
[10]P. Gosar and L. Vilfan, Mol. Phys. **18**, 49 (1970).
[11]L. Vilfan, *Organic Conductors and Semiconductors,* Lecture Notes in Physics Vol. 65 (Springer-Verlag, Berlin, 1977), p. 629.
[12]H. Sumi, Solid State Commun. **28**, 309 (1978).
[13]V. Ern, A. Suna, Y. Tomkievicz, P. Avakian, and R. P. Groff, Phys. Rev. B **5**, 3222 (1972).
[14]V. Ern, Phys. Rev. Lett. **22**, 343 (1969).
[15]G. Durocher and D. F. Williams, J. Chem. Phys. **51**, 1675 (1969).
[16]D. C. Hoestery and G. W. Robinson, J. Chem. Phys. **54**, 1709 (1971).
[17]J. Jortner, S. A. Rice, J. L. Katz, and S. Choi, J. Chem. Phys. **42**, 309 (1965).
[18]C. E. Swenberg, J. Chem. Phys. **51**, 1753 (1968).
[19]A. Tiberghien and G. Delacôte, J. Phys. **31**, 637 (1970).
[20]R. Mason, Acta Crystallogr. **17**, 547 (1964).
[21]D. W. J. Cruickshank, Acta Crystallogr. **9**, 915 (1956).
[22]D. E. Williams, J. Chem. Phys. **47**, 4680 (1967).
[23]D. W. J. Cruickshank, Acta Crystallogr. **10**, 470 (1957).
[24]K. Yokoi and W. Siebrand, J. Chem. Phys. **92**, 7636 (1990).
[25]E. Clementai and C. C. J. Roothaan, Phys. Rev. **127**, 1618 (1962).
[26]E. F. McCoy and I. G. Ross, Aust. J. Chem. **4**, 573 (1962).
[27]S. I. Choi, J. Jortner, S. A. Rice, and R. Silbey, J. Chem. Phys. **41**, 3294 (1964).
[28]G. Durocher and D. F. Williams, J. Chem. Phys. **51**, 5405 (1969).
[29]L. Sebastian, G. Weiser, G. Peter, and H. Bässler, Chem. Phys. **75**, 103 (1983).
[30]W. Siebrand, B. Ries, and H. Bässler, J. Mol. Electron. **3**, 113 (1987).
[31]L. B. Schein, Chem. Phys. Lett. **48**, 571 (1977).
[32]L. B. Schein, Phys. Rev. B **15**, 1024 (1977).
[33]P. J. Reucroft, A. R. McGhie, E. E. Hillman, and V. V. Damiano, J. Cryst. Growth **11**, 355 (1971).
[34]E. A. Silinsh, *Organic Molecular Crystals* (Springer-Verlag, Berlin, 1980), p. 154.
[35]R. G. Della Valle, F. Zerbetto, A. Brillante, and K. Syassen, J. Lumin. **38**, 311 (1987).
[36]V. D. Haaer and H. C. Wolf, Mol. Cryst. Liq. Cryst. **10**, 359 (1970).
[37]H. Kolb and H. C. Wolf, Z. Natürforsch. A **27**, 51 (1972).
[38]K. V. Burg, L. Altwegg, and I. Z. Granacher, Phys. Rev. B **22**, 2037 (1980).
[39]K. Yokoi and Y. Ohba, J. Chem. Phys. **87**, 1887 (1987).